Taking advantage of multiple solutions in configuration-dependent substructure decoupling

J. Brunetti [1], **W. D'Ambrogio** [1], **A. Fregolent** [2]
[1] Università degli Studi dell'Aquila,
DIIIE - Dipartimento di Ingegneria Industriale dell'Informazione e di Economia
Piazzale Ernesto Pontieri 1, Monteluco di Roio, I-67100 L'Aquila (AQ), Italy
e-mail: **jacopo.brunetti@univaq.it**

[2] Università di Roma La Sapienza, Dipartimento di Ingegneria Meccanica e Aerospaziale,
Via Eudossiana 18, I-00184 Roma, Italy

Abstract
Substructure decoupling allows identifying the unknown dynamic behavior of a subsystem starting from the dynamic behavior of both the whole system and the residual part of the system. Substructuring techniques were originally developed to deal with invariant systems. The feasibility of performing substructure decoupling when the coupling conditions among invariant mechanical subsystems are configuration-dependent was recently investigated. Typical examples of such systems could be a lifting crane or a cartesian robot. In principle, when the unknown subsystem is identified by performing substructure decoupling on different configurations of the assembled system, one would expect to get the same solution. In practice, this is not true because the decoupling problem may be affected by ill-conditioning that depends on the configuration of the assembled system. In this work, the redundancy of information provided by multiple solutions is exploited through different strategies to reduce the effects of ill-conditioning.

1 Introduction

When a complex dynamic system ideally composed by a set of connected subsystems is considered, substructure decoupling allows identifying the unknown dynamic behavior of a subsystem starting from the dynamic behavior of both the whole system and the residual part of the system. Substructuring techniques were originally developed to deal with invariant systems [1, 2, 3, 4].

In a recent work [5], the authors investigated the feasibility of performing substructure decoupling when the coupling conditions among invariant mechanical subsystems are configuration-dependent. Typical examples of such systems are a lifting crane or a Cartesian robot. The dynamic behavior of the whole system must be known for each configuration, but it is assumed that only coupling conditions are configuration dependent, i.e. the component subsystems are invariant. Therefore, the use of multiple configurations can provide a more rich set of information that can improve the identification of the unknown (invariant) subsystem. Moreover, in substructure decoupling it is not required to know the dynamic behavior of the assembled system at the connecting DoFs between the component subsystems [6, 7].

On the contrary, the classical coupling problem in the framework of experimental dynamic substructuring always requires to know the dynamic behavior of the subsystems to be coupled at the connecting DoFs, either directly or using reduction techniques or introducing additional subsystems [8, 9, 10]. Also the coupling problem can be considered for configuration dependent systems [11, 12, 13, 14]: this allows to investigate friction-induced vibrations in the framework of dynamic substructuring [15, 16].

Going back to configuration-dependent substructure decoupling, the results [5] showed that it is possible to identify an appropriate set of measuring points, which allows both to avoid taking measurements on the coupling points and to use a single set of measured FRFs on the residual subsystem. In principle, when

the unknown subsystem is identified by performing substructure decoupling on different configurations of the assembled system, one would expect to get the same solution. In practice, this is not true because the decoupling problem may be affected by ill-conditioning or by specific noise sources that depends on the configuration of the assembled system [2, 3, 7, 17, 18].

In this paper, different strategies are conceived to exploit the redundancy provided by the multiple solutions, obtained by solving the decoupling problem in different configurations. Results are obtained starting from simulated noise polluted FRFs on a well known test bed [6, 7].

2 Decoupling of structural system with multiple configurations

Typically, substructure decoupling allows identifying the unknown dynamic behavior of a subsystem, starting from the dynamic behavior (e.g., FRFs) of the assembled system RU and that of a known portion of it, the so-called residual subsystem R. A set of coupled systems made by a pair of invariant substructures joined at different DoFs is considered. Each coupled system in the set is defined as *configuration*. For a given configuration χ, the unknown substructure U (N_U DoFs) is joined to the residual substructure R (N_R DoFs) by n_c coupling DoFs through which constraint forces (and moments) are exchanged (see Figure 1). The degrees of freedom of each assembled structure (N_{RU} DoFs) can be partitioned into coupling DoFs (c), internal DoFs of substructure U (u) and internal DoFs of substructure R (r), that are generally different for each configuration χ.

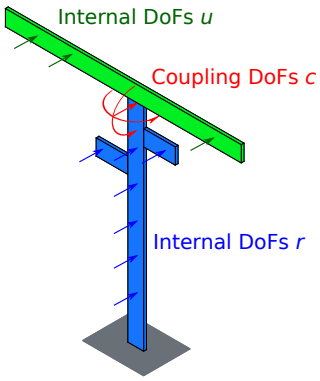

Figure 1: Assembled system RU, with the unknown subsystem U (green) and the residual subsystem R (blue).

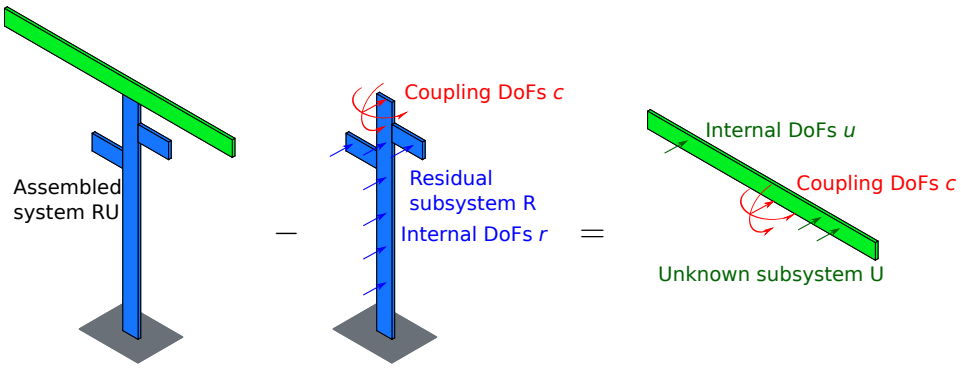

Figure 2: Scheme of the direct decoupling problem.

The FRFs of the unknown subsystem U can be predicted from those of a given assembled system RU_χ by subtracting the dynamics of the residual subsystem R. This is accomplished by adding to a given assembled system RU_χ a fictitious subsystem (negative structure) with a dynamic stiffness opposite to that of the invariant residual subsystem R (see Figure 2). The effect of the negative system is to add disconnection forces (and moments) to the external forces acting on the assembled system RU_χ to uncouple the unknown subsystem from the assembled system.

The dynamic equilibrium of a given assembled system RU_χ is expressed as:

$$\mathbf{Z}_\chi^{RU} \boldsymbol{u}_\chi^{RU} = \boldsymbol{f}_\chi^{RU} + \boldsymbol{g}_\chi^{RU} \tag{1}$$

where $\boldsymbol{g}_\chi^{RU}$ is the vector of disconnection forces applied to the given assembled system by the negative subsystem, $\mathbf{Z}_\chi^{RU}$ is the dynamic stiffness matrix of the given assembled system RU_χ, $\boldsymbol{u}_\chi^{RU}$ is the vector of degrees of freedom of the given assembled system RU_χ, $\boldsymbol{f}_\chi^{RU}$ is the external force vector on the assembled system RU_χ.

Similarly, the dynamic equilibrium of the negative subsystem is expressed as:

$$-\mathbf{Z}^R \boldsymbol{u}_\chi^R = \boldsymbol{f}_\chi^R + \boldsymbol{g}_\chi^R \tag{2}$$

where $-\mathbf{Z}^R$ is the dynamic stiffness matrix of the invariant negative subsystem, and $\boldsymbol{u}_\chi^R$, $\boldsymbol{f}_\chi^R$, $\boldsymbol{g}_\chi^R$ are defined as for the assembled system.

2.1 Possible sets of interface DoFs

The DoFs on which the disconnection forces are acting constitute the set of interface DoFs. This set is not unique even for a given configuration χ [6].

Equations (1-2) can be coupled to obtain the unknown subsystem U, by enforcing the following constraints: disconnection forces $\boldsymbol{g}_\chi^{RU}$ and $\boldsymbol{g}_\chi^R$ must be in equilibrium, and compatibility between degrees of freedom $\boldsymbol{u}_\chi^{RU}$ and $\boldsymbol{u}_\chi^R$ must hold at the interface between the assembled system RU_χ and the negative subsystem.

A possible set of disconnection forces trivially consists of forces and moments acting at the coupling DoFs and opposite to the constraint forces and moments (see Fig. 3), giving rise to the:

- standard interface, including only the coupling DoFs (c) between subsystems U and R.

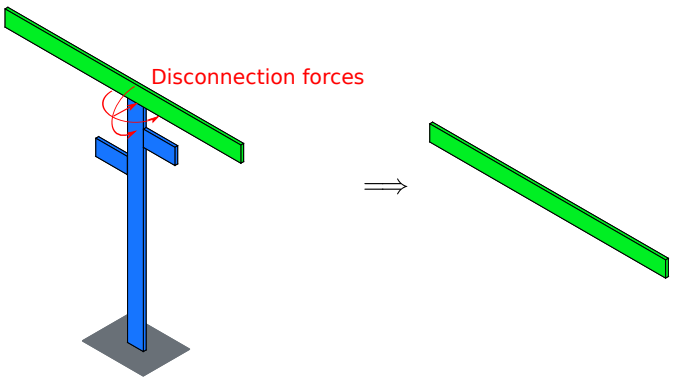

Figure 3: Trivial set of disconnection forces (and moments) acting on the assembled structure (corresponding to the standard interface).

It is possible to consider also non trivial sets of disconnection forces, acting at different DoFs but still able to cancel the constraint forces and moments at the coupling DoFs (see Fig. 4). Therefore, several other options for interface DoFs can be considered:

- extended interface, including also a subset of internal DoFs ($i \subseteq r$) of subsystem R;
- mixed interface, including subsets of coupling DoFs ($d \subset c$) and internal DoFs ($i \subseteq r$), e.g. those corresponding to the disconnection forces in Fig. 4 (left);
- pseudo interface, including only internal DoFs ($i \subseteq r$) of subsystem R, e.g. those corresponding to the disconnection forces in Fig. 4 (rigth).

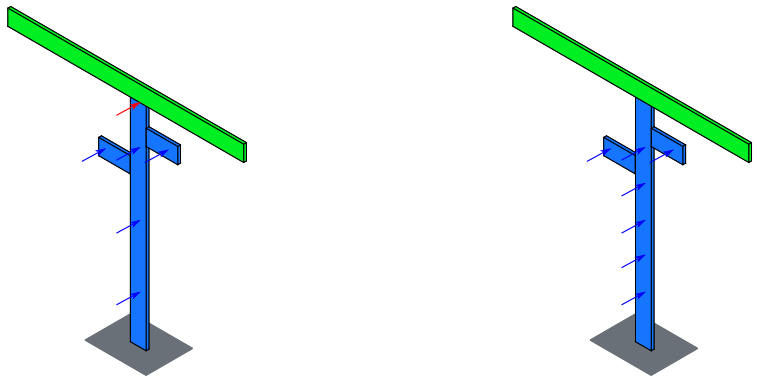

Figure 4: Non-trivial sets of disconnection forces corresponding to a mixed interface (left) and to a pseudo interface (right).

In any case, the number of interface DoFs must be not less than the number of coupling DoFs n_c. The use of a mixed interface can be useful to replace rotational coupling DoFs with internal DoFs, whilst the use of a pseudo interface allows to replace all the coupling DoFs with translational internal DoFs.

2.2 Compatibility and equilibrium for a given configuration

Compatibility at the (standard, extended, mixed, pseudo) interface implies that any pair of matching DoFs, i.e. DoF l on the coupled system RU_χ and DoF m on subsystem R, must have the same displacement, that is $u_l^{RU} - u_m^R = 0$. Let S_χ be the set of N_χ interface DoFs on which compatibility is enforced.

For a given configuration χ, the compatibility condition can be generally expressed as:

$$\mathbf{B}_\chi \boldsymbol{u}_\chi = \mathbf{0} \qquad \text{where} \qquad \boldsymbol{u}_\chi = \begin{Bmatrix} \boldsymbol{u}_\chi^{RU} \\ \boldsymbol{u}_\chi^{R} \end{Bmatrix} \tag{3}$$

where $\mathbf{B}_\chi$ has size $N_\chi \times (N_{RU} + N_R)$ and each row corresponds to a pair of matching DoFs.

The equilibrium condition can be enforced on the same set S_χ of N_χ interface DoFs used for compatibility condition [3]. The equilibrium condition implies that the sum of disconnection forces on any pair of matching DoFs must be zero that is $g_l^{RU} + g_m^R = 0$. Furthermore, for any unmatched DoF k on the coupled system RU_χ (or on the residual subsystem R), it must be $g_k^{RU} = 0$ ($g_k^R = 0$). Altogether, the previous conditions can be expressed as:

$$\mathbf{L}_\chi^T \boldsymbol{g}_\chi = \mathbf{0} \qquad \text{where} \qquad \boldsymbol{g}_\chi = \begin{Bmatrix} \boldsymbol{g}_\chi^{RU} \\ \boldsymbol{g}_\chi^{R} \end{Bmatrix} \tag{4}$$

where $\mathbf{L}_\chi$ is a localization matrix and has size $(N_{RU} + N_R) \times (N_{RU} + N_R - N_\chi)$.

2.3 Formulation of the decoupling problem for a given configuration

The problem to be solved is mathematically built by gathering Eqs. (1-4). The solution is obtained using a dual assembly [8, 2] where equilibrium is satisfied exactly by defining a unique set of disconnection force intensities but compatibility could not be ensured.

In the dual assembly, the total set of DoFs is retained, and the equilibrium condition $g_r^{RU} + g_s^R = 0$ at a pair of matching DoFs is ensured by choosing $g_r^{RU} = -\lambda_r$ and $g_s^R = \lambda_r$. Therefore, the overall interface equilibrium can be ensured by writing the disconnection forces in the form:

$$\boldsymbol{g}_\chi = -\mathbf{B}_\chi^T \boldsymbol{\lambda}_\chi \tag{5}$$

where $\boldsymbol{\lambda}_\chi$ is a vector of Lagrange multipliers corresponding to disconnection force intensities.

Since there is a unique disconnection force intensity λ_r for any pair of equilibrium DoFs, Eq. (4) is satisfied automatically for any $\boldsymbol{\lambda}_\chi$.

Therefore, Eqs. (1–3) become, after substituting Eq. (5) into Eqs. (1–2) recast in matrix form:

$$\begin{cases} \mathbf{Z}_\chi \boldsymbol{u}_\chi + \mathbf{B}_\chi^T \boldsymbol{\lambda}_\chi = \boldsymbol{f}_\chi & (6) \\ \mathbf{B}_\chi \boldsymbol{u}_\chi = \mathbf{0} & (7) \end{cases}$$

where $\mathbf{Z}_\chi$ is obtained by gathering the dynamic stiffness of the assembled system and that of the residual subsystem in block diagonal format as $\text{diag}(\mathbf{Z}_\chi^{RU}, -\mathbf{Z}^R)$, and $\boldsymbol{f}_\chi$ is defined similarly to $\boldsymbol{g}_\chi$ in Eq.(4).

To obtain the disconnection force intensities $\boldsymbol{\lambda}_\chi$, displacements $\boldsymbol{u}_\chi$ can be obtained from Eq. (6) and substituted into Eq. (7). Then, by defining the FRF block diagonal matrix:

$$\mathbf{H}_\chi = \mathbf{Z}_\chi^{-1} = \begin{bmatrix} \mathbf{H}_\chi^{RU} & 0 \\ 0 & -\mathbf{H}^R \end{bmatrix} \tag{8}$$

the vector of disconnection force intensities $\boldsymbol{\lambda}_\chi$ is found as:

$$\boldsymbol{\lambda}_\chi = \left(\mathbf{B}_\chi \mathbf{H}_\chi \mathbf{B}_\chi^T\right)^{-1} \mathbf{B}_\chi \mathbf{H}_\chi \boldsymbol{f}_\chi \tag{9}$$

The FRF of the unknown subsystem U can be obtained by back-substituting $\boldsymbol{\lambda}_\chi$ in Eq. (6), and by isolating $\boldsymbol{u}_\chi$ at the left hand side:

$$\boldsymbol{u}_\chi = \left(\mathbf{H}_\chi - \mathbf{H}_\chi \mathbf{B}_\chi^T \left(\mathbf{B}_\chi \mathbf{H}_\chi \mathbf{B}_\chi^T\right)^{-1} \mathbf{B}_\chi \mathbf{H}_\chi\right) \boldsymbol{f}_\chi \tag{10}$$

which is in the form $\boldsymbol{u}_\chi = \widetilde{\mathbf{H}}_\chi \boldsymbol{f}_\chi$, so that the FRF of the unknown subsystem $\mathbf{H}_\chi^U$ is a portion of:

$$\widetilde{\mathbf{H}}_\chi = \mathbf{H}_\chi - \mathbf{H}_\chi \mathbf{B}_\chi^T \left(\mathbf{B}_\chi \mathbf{H}_\chi \mathbf{B}_\chi^T\right)^{-1} \mathbf{B}_\chi \mathbf{H}_\chi \tag{11}$$

In fact, when using the dual assembly, the rows and the columns of $\widetilde{\mathbf{H}}_\chi$ corresponding to compatibility and equilibrium DoFs appear twice. Furthermore, when using an extended, mixed or pseudo interface, the rows and columns of $\widetilde{\mathbf{H}}_\chi$ corresponding to the internal DoFs of the residual substructure R are meaningless. Therefore, only meaningful and independent entries are retained in $\mathbf{H}_\chi^U$. In Eq. (11), the matrix to be inverted is known as interface flexibility matrix; it depends on the choice of interface DoFs and it can be ill-conditioned for some set of interface DoFs.

2.4 Taking full advantage of different configurations

Since the unknown subsystem is the same in any configuration, $\mathbf{H}_\chi^U$ should remain the same as the configuration changes. Although this is true in principle, in practice some differences can arise due to both numerical issues and noise in experimental FRFs. The different solutions can be exploited to gain a better understanding of the dynamic behavior of the unknown subsystem. Several approaches are possible to take advantage of the redundancy of solutions:

- Observation and assessment
- Averaging

2.4.1 Observation and assessment of different solutions

The decoupling problem can be solved independently for each configuration of the coupled system, following the classical decoupling approach outlined in section 2.3. If the same pseudo interface is considered for all configurations, the same set of measurement of the residual structure can be used. Often, when dealing with experimental measurements, the noise can affect in different way the quality of the decoupling results. Sometimes, it is possible to observe high scatter only in some solutions and in limited frequency bands. Having multiple solutions, one could consider only the best results in each frequency band. However when it is not easy to identify the best results, methods not relying on individual judgment are also necessary.

2.4.2 Arithmetic average

The decoupling solutions obtained using different configurations can be put together by performing an arithmetic average of the FRFs of the unknown substructure:

$$\mathbf{H}^U = \frac{1}{N}\sum_{\chi=1}^{N}\mathbf{H}_\chi^U \tag{12}$$

2.4.3 Weighted average

A careful observation of the solutions obtained using different configurations might suggest that the FRFs of the unknown susbsystem should be averaged using weights that depend on the quality of the FRF:

$$\mathbf{H}^U(\omega) = \sum_{\chi=1}^{N} w_\chi(\omega)\mathbf{H}_\chi^U(\omega) \tag{13}$$

A high value of the scatter $\gamma_\chi(\omega)$ of each FRF can be used as an indicator of the low quality of the solution in the neighborhood of each frequency. Therefore, the weight $w_\chi(\omega)$ is defined in order to be inversely proportional to the scatter and is normalized so that $\sum_\chi w_\chi(\omega) = 1$:

$$w_\chi(\omega) = \frac{\gamma_\chi^{-1}(\omega)}{\sum_{\chi=1}^{N}\gamma_\chi^{-1}(\omega)} \tag{14}$$

The scatter level γ_χ around a given frequency ω can be evaluated using the moving variance, computed over a short sliding window of k frequency samples. The scatter of several quantities can be observed, e.g., the log modulus, the phase, or the complex value of the FRFs. More specifically, the following quantities are considered here to estimate the scatter:

- logarithm of the FRF modulus:

$$\gamma_\chi(\omega) = \tilde{\sigma}_k^2\Big(\log\big(|H_\chi(\omega)|\big)\Big) \tag{15}$$

  where $\tilde{\sigma}_k^2(g(\omega))$ represents the moving variance of the function $g(\omega)$ using a sliding windows of k frequency samples.

- logarithm of the complex value of the FRF:

$$\gamma_\chi(\omega) = \tilde{\sigma}_k^2\Big(\log\big(H_\chi(\omega)\big)\Big) \tag{16}$$

  With this approach results are similar to those obtained with the logarithm of the FRF modulus.

- phase of the FRF:

$$\gamma_\chi(\omega) = \tilde{\sigma}_k^2\Big(\varphi\big(H_\chi(\omega)\big)\Big) \tag{17}$$

3 Model and results

In order to investigate how to take advantage of configuration dependent substructure decoupling, a previously introduced [6] test bed is considered. The assembled system consists of a cantilever beam with two short arms (the residual subsystem R) bolted to a beam (unknown subsystem U), shown in Figure 5. The joint involves both translational and rotational DoFs. The cross section is 40 mm$\times$8 mm for all beams, with the short side along the z-direction. The subsystem geometrical dimension are shown in Table 1(a).

Three different configurations of the assembly are obtained by connecting the residual and the unknown subsystems at three different points. Figure 6 shows the configurations of the assembly considered in this paper and Table 1(b) shows the configuration dependent geometrical dimensions. Furthermore, Table 2 lists the coupling and the internal DoFs for the considered configurations.

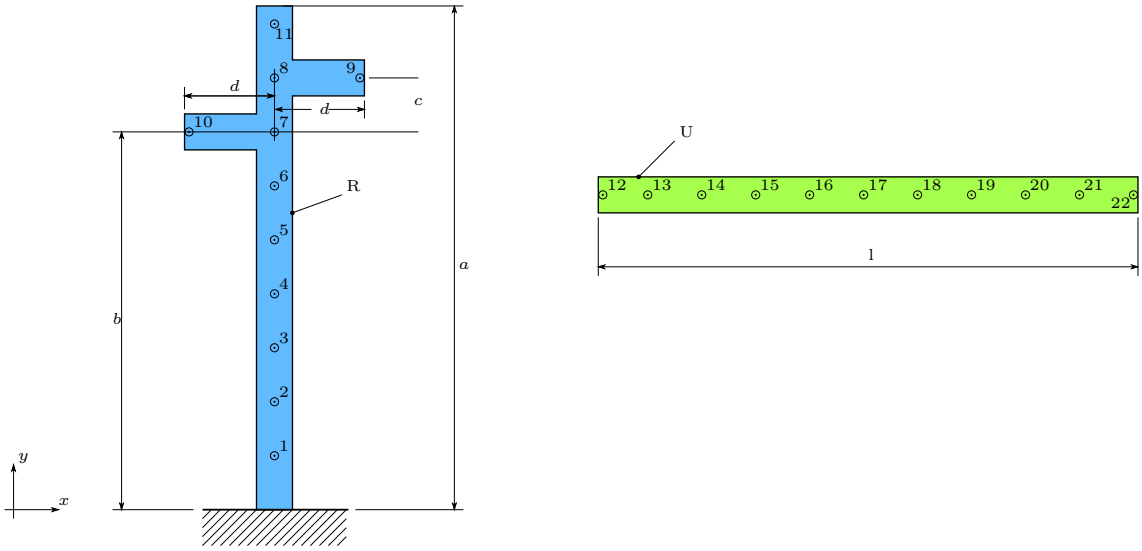

Figure 5: Sketch of the residual subsystem R (left) and of the unknown subsystem U (right).

Table 1: Geometrical dimensions [mm]

(a) Invariant dimensions

a	b	c	d	l
540	420	60	100	600

(b) Configuration-dependent dimensions

Configuration	e	h
A	240	540
B	240	360
C	180	540

Tu simulate real world data, the FRFs of the assembled systems and of the residual subsystem R, obtained using the numerical models, are polluted with 0.2% noise.

Figure 7 shows the drive point inertance for DoF 16z of the unknown subsystem U evaluated considering the three different configurations. The results show that, up to a frequency of about 600 Hz, the dynamics is consistently estimated by the three considered configuration, but above 600 Hz the estimations show large discrepancies. Among the three considered configurations of the assembly, the configuration C seems to provide the less scattered FRF in the frequency band 650–850 Hz.

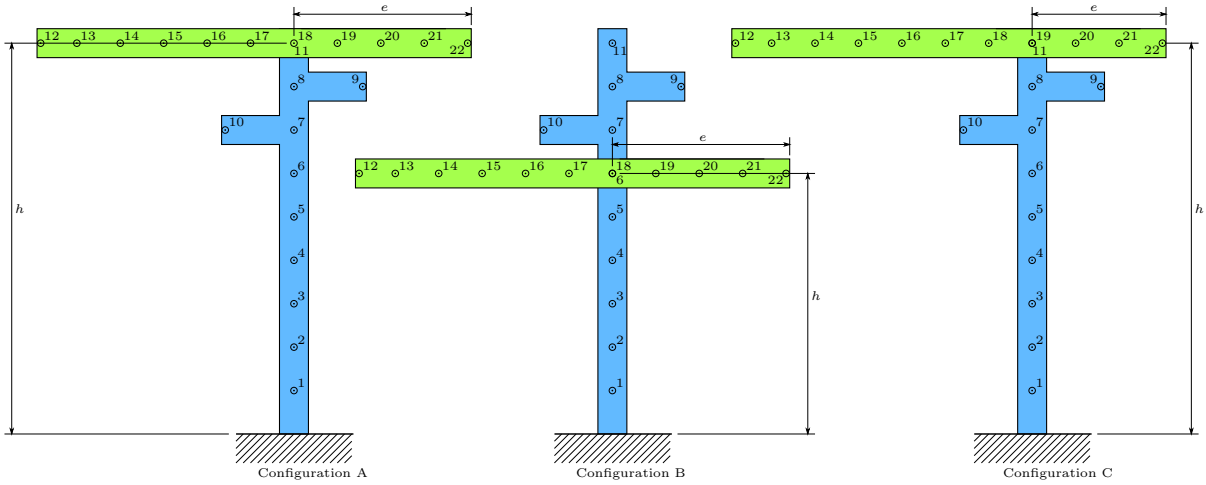

Figure 6: Sketch of assembled system in different configurations.

Table 2: Coupling and internal DoFs for the residual R and the unknown U subsystems for the three considered configurations of the assembly.

Configuration	Coupling DoF R	Coupling DoF U	Internal DoFs R	Internal DoFs U
A	11	18	1:10	[12:17, 19:22]
B	6	18	[1:5, 7:11]	[12:17, 19:22]
C	11	19	1:10	[12:18, 20:22]

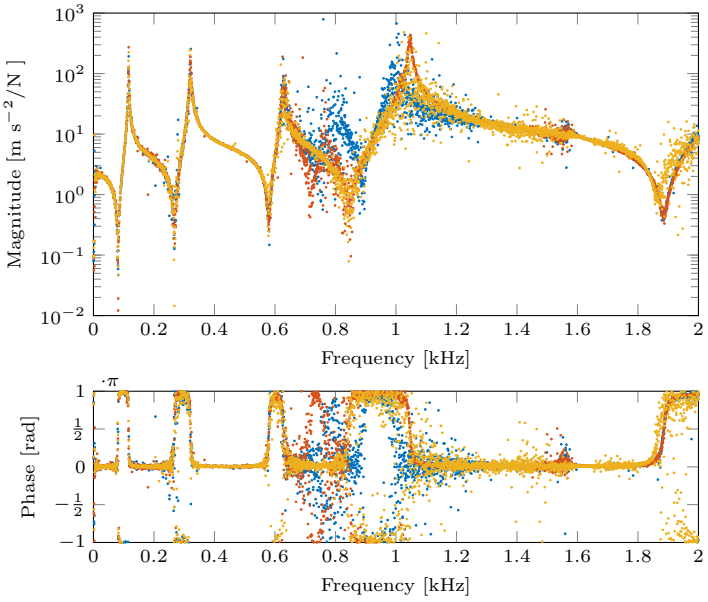

Figure 7: $H_{16z,16z}$ of the unknown subsystem for different configurations. Configuration A (·····); Configuration B (·····); Configuration C (·····)

To exploit the contributions of different configurations, the procedures outlined in section 2.4 are used.

Using the arithmetic average, the results shown in Figure 7 are processed as indicated in Eq. (12). The result is shown in Figure 8, compared with the exact FRF provided by the numerical model. As expected, the arithmetic average is able to attenuate the errors introduced by a single configuration, but it cannot be considered an optimal approach since wrong contributions are mitigated but not eliminated.

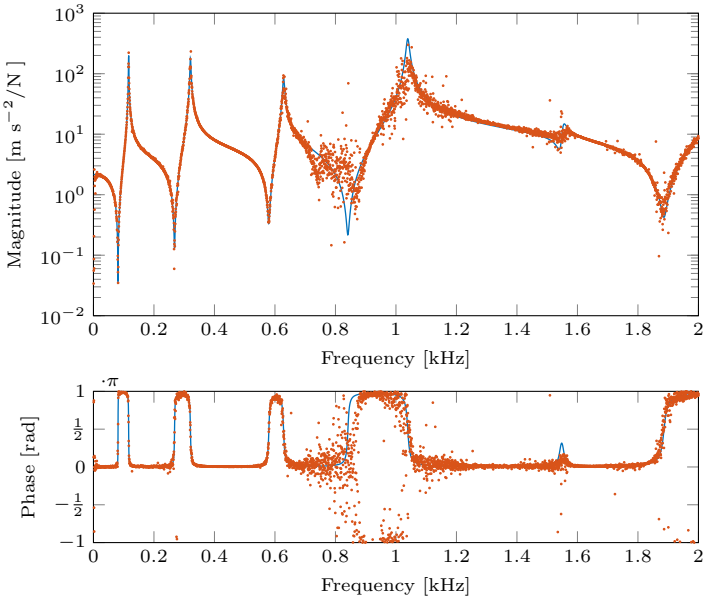

Figure 8: $H_{16z,16z}$ obtained as arithmetic average of the solutions in Figure 7. Reference (——); Arithmetic average (·····).

Using the weighted average, the results shown in Figure 7 are processed as indicated in Eq. (13) using the weights defined in Eq. (14). The scatter level γ_χ is evaluated using the moving variance of the log modulus, of the logarithm of the complex value, or the phase of the FRF, computed over a sliding window of k=5 frequency samples.

Using the logarithm of the FRF modulus, as defined in Eq. (15), the results are those in Figure 9. It can be noticed that the estimated FRF is quite improved with respect to the one provided by arithmetic average.

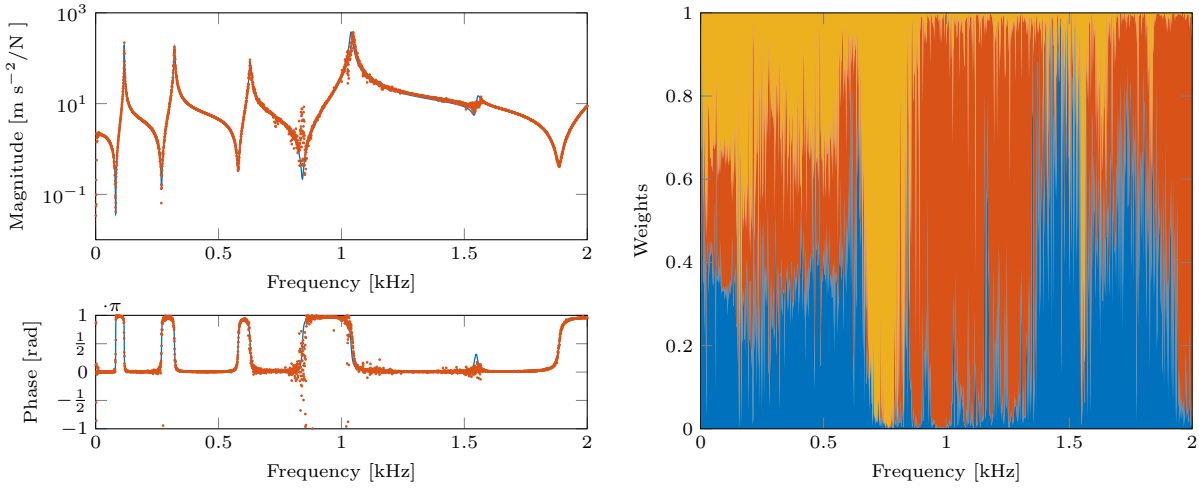

Figure 9: Left. $H_{16z,16z}$ obtained as weighted average using the moving variance of the logarithm of the FRF modulus. Reference (——); Weighted average (·····). Right. Stacked plot of the weights of the different configurations: Configuration A ■ (blue); Configuration B ■ (red); Configuration C ■ (yellow).

This happens because in this case the weights are chosen in a smart way, differently from the case of the arithmetic average where they are all equal to 1/3.

Using the logarithm of the complex value of the FRF, as defined in Eq. (16), the results are those in Figure 10. Also in this case, the estimated FRF is quite improved with respect to the one provided by arithmetic average. Furthermore, the estimated FRF is very similar to the one obtained by using the logarithm of the FRF modulus.

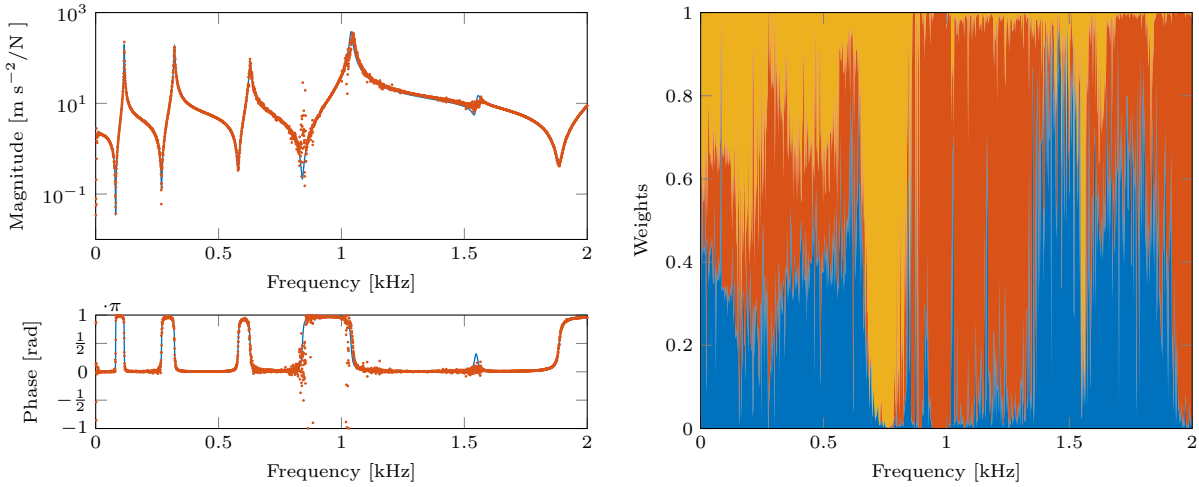

Figure 10: Left. $H_{16z,16z}$ obtained as weighted average using the moving variance of the logarithm of the complex value of the FRF. Reference (——); Weighted average (·····). Right. Stacked plot of the weights of the different configurations: Configuration A ■ (blue); Configuration B ■ (red); Configuration C ■ (yellow).

Using the phase of the FRF, as defined in Eq. (17), the results are those in Figure 11. Again, the estimated FRF is quite improved with respect to the one provided by arithmetic average and is very similar to the ones obtained by using either the logarithm of the modulus or the logarithm of the complex value of the FRF. In fact, the weights computed using the scatter of the log FRF modulus, the log FRF value and the FRF phase are quite similar because these different quantities are likewise able to account for the quality of the considered solutions.

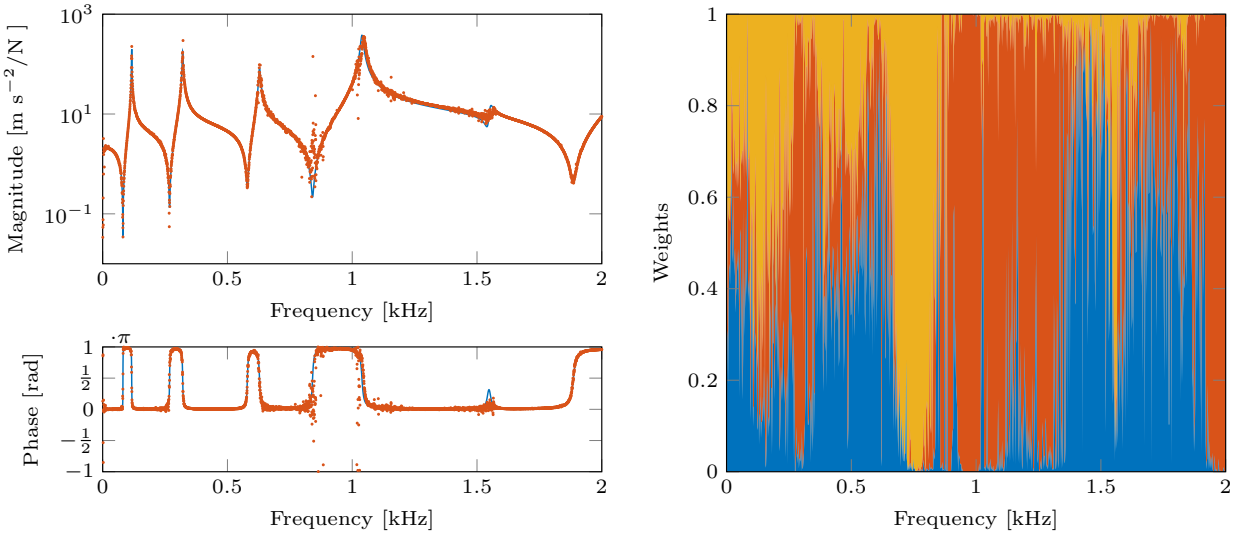

Figure 11: $H_{16z,16z}$ obtained as weighted average using the moving variance of the phase of the FRF. Reference (——); Weighted average (·····). Right. Stacked plot of the weights of the different configurations: Configuration A ■ (blue); Configuration B ■ (red); Configuration C ■ (yellow).

4 Conclusions

In this paper, the decoupling procedure is applied to configuration dependent systems composed by invariant mechanical subsystems with configuration dependent coupling conditions. Specifically, a system composed by two invariant substructures assembled in three different configurations is considered. The decoupling procedure is performed to identify the same unknown subsystem, assembled in different configurations. Under these conditions the only difference introduced in the decoupling formulation by the configuration is the FRF matrix of the assembled structure.

The decoupling problem is solved independently for each considered configuration, obtaining several estimations of the FRF of the unknown subsystem. Although the unknown structure is always the same, the different estimations of the FRF can have some discrepancies. In particular, some FRFs can show higher levels of scatter in some frequency bands. Therefore, several strategies are used to exploit the redundancy of information deriving from the multiple configurations of the assembled system. The results, obtained using simulated noise polluted FRFs, highlight that the arithmetic average of the solutions is not particularly advantageous, because possible outliers are averaged but not eliminated. On the contrary, weighted averages, where frequency dependent weights are inversely proportional to the scatter of FRF related quantities, allow to obtain significant improvement in the final estimation of the FRF the unknown subsystem. Further developments will consider using experimentally determined FRFs.

Acknowledgements

This research is supported by University of Rome La Sapienza and University of L'Aquila.

References

[1] P. Sjövall and T. Abrahamsson, "Substructure system identification from coupled system test data," *Mech. Syst. Sig. Process.*, vol. 22, no. 1, pp. 15–33, 2008.

[2] W. D'Ambrogio and A. Fregolent, "The role of interface DoFs in decoupling of substructures based on the dual domain decomposition," *Mech. Syst. Sig. Process.*, vol. 24, no. 7, pp. 2035–2048, Oct. 2010.

[3] S. N. Voormeeren and D. J. Rixen, "A family of substructure decoupling techniques based on a dual assembly approach," *Mech. Syst. Sig. Process.*, vol. 27, pp. 379–396, Feb 2012.

[4] W. D'Ambrogio and A. Fregolent, "Inverse dynamic substructuring using direct hybrid assembly in the frequency domain," *Mech. Syst. Sig. Process.*, vol. 45, no. 2, pp. 360–377, 2014.

[5] J. Brunetti, W. D'Ambrogio, and A. Fregolent, "Feasibility of configuration-dependent substructure decoupling," in *Dynamic Substructures, Volume 4*, M. S. Allen, W. D'Ambrogio, and D. Roettgen, Eds. Cham: Springer International Publishing, 2022.

[6] W. D'Ambrogio and A. Fregolent, "Substructure decoupling without using rotational dofs: Fact or fiction?" *Mech. Syst. Sig. Process.*, vol. 72-73, pp. 499 – 512, 2016.

[7] W. D'Ambrogio and A. Fregolent, "Replacement of unobservable coupling dofs in substructure decoupling," *Mech. Syst. Sig. Process.*, vol. 95, pp. 380 – 396, Oct 2017.

[8] D. de Klerk, D. J. Rixen, and S. Voormeeren, "General framework for dynamic substructuring: History, review, and classification of techniques," *AIAA Journal*, vol. 46, no. 5, pp. 1169–1181, May 2008.

[9] D. Rixen, "A dual Craig-Bampton method for dynamic substructuring," *J. Comput. Appl. Math.*, vol. 168, no. 1-2, pp. 383–391, 2004, cited By 156.

[10] R. L. Mayes and M. R. Ross, "Advancements in hybrid dynamic models combining experimental and finite element substructures," *Mech. Syst. Sig. Process.*, vol. 31, pp. 56 – 66, 2012.

[11] T. Semm, M. B. Nierlich, and M. F. Zaeh, "Substructure Coupling of a Machine Tool in Arbitrary Axis Positions Considering Local Linear Damping Models," *J. Manuf. Sci. Eng.*, vol. 141, no. 7, 05 2019, 071014.

[12] T. Semm, C. Rebelein, and M. Zaeh, "Prediction of the position dependent dynamic behavior of a machine tool considering local damping effects," *CIRP J. Manuf. Sci. Technol.*, vol. 27, pp. 68 – 77, 2019.

[13] L. Carassale, P. Silvestri, R. Lengu, and P. Mazzaron, "Modeling rail-vehicle coupled dynamics by a time-varying substructuring scheme," in *Dynamic Substructures, Volume 4*, A. Linderholt, M. S. Allen, R. L. Mayes, and D. Rixen, Eds. Cham: Springer International Publishing, 2020, pp. 167–171.

[14] J. Brunetti, W. D'Ambrogio, and A. Fregolent, "Dynamic coupling of substructures with sliding friction interfaces," *Mech. Syst. Sig. Process.*, vol. 141, 2020.

[15] J. Brunetti, W. D'Ambrogio, and A. Fregolent, "Friction-induced vibrations in the framework of dynamic substructuring," *Nonlinear Dyn.*, vol. 103, no. 4, pp. 3301–3314, 2021.

[16] J. Brunetti, W. D'Ambrogio, and A. Fregolent, "Evaluation of different contact assumptions in the analysis of friction-induced vibrations using dynamic substructuring," *Machines*, vol. 10, no. 5, 2022.

[17] P. Peeters, S. Manzato, T. Tamarozzi, and W. Desmet, "Reducing the impact of measurement errors in FRF-based substructure decoupling using a modal model," *Mech. Syst. Sig. Process.*, vol. 99, pp. 384–402, 2018.

[18] F. Trainotti, T. Bregar, S. Klaassen, and D. Rixen, "Experimental decoupling of substructures by singular vector transformation," *Mech. Syst. Sig. Process.*, vol. 163, 2022.